2023-10

Geochronology, Mineralogy, and Geochemistry of the Tonsteins from the PermoCarboniferous Benxi Formation, Ordos Basin, North China Craton

WANG, L

10.1111/1755-6724.15063
Acta Geologica Sinica - English Edition
Wiley

Geochronology, Mineralogy, and Geochemistry of the Tonsteins from the Permo-Carboniferous Benxi Formation, Ordos Basin, North China Craton

WANG Luojing[1], LV Dawei[1], ZHANG Zhihui[1, *], James C. HOWER[2], Munira RAJI[3], ZHANG Yushuai[1], SHEN Yangyang[1] and GAO Jie[1]

[1] *Shandong Provincial Key Laboratory of Depositional Mineralization and Sedimentary Minerals, College of Earth Sciences and Engineering, Shandong University of Science and Technology, Qingdao 266590, China*
[2] *University of Kentucky, Center for Applied Energy Research, 2540 Research Park Drive, Lexington, KY 40511, United States of America*
[3] *Sustainable Earth Institute, University of Plymouth, Devon PL4 8AA, UK*

Abstract: Tonstein layers are found worldwide in the Permo-Carboniferous coal-bearing strata. This study investigates the geochronology, mineralogy, and geochemistry of four tonstein samples from the Permo-Carboniferous Benxi Formation, Ordos Basin, North China Craton (NCC). The typical features of the studied tonsteins include thin beds, lateral continuity, angular quartz grains, and euhedral zircons with similar U–Pb ages, indicating a significant pyroclastic origin. In addition, the tonstein samples have low TiO_2/Al_2O_3 ratios (< 0.02) and rare earth elements and yttrium (REY) concentrations with obvious negative Eu anomalies, indicating that the tonsteins have a felsic magma origin. Moreover, compared with the mean composition of clay shale, the studied tonsteins are characterized by high concentrations of the elements Nb and Ta, which may affect the concentration of the corresponding elements in surrounding coal seams. The zircon U–Pb ages of the tonsteins (293.9–298.8 Ma) provide a precise chronological framework on the Benxi Formation in the Ordos Basin, constraining the Gzhelian-Aselian stages. The tonsteins were probably sourced from arc volcanism along the western margin of the NCC during the Early Permian, implying that the Alxa Terrane had not amalgamated with the NCC at that time.

Key words: Permo-Carboniferous, tonsteins, geochemistry, North China Craton

* Corresponding author. E-mail: zhzhihui@sdust.edu.cn

1 Introduction

Many altered volcanic ashes (tonstein) have been observed in coal seams (Dai et al., 2017 and references therein; Zhang et al., 2022), occurring mainly as thin but laterally persistent layers (Bohor and Triplehorn, 1993; Dai et al., 2011, 2017; Spears, 2012; Spears and Arbuzov, 2019). These tonsteins are significant for global chronostratigraphic calibration and correlation. As some primary minerals that survived weathering and post-depositional alteration in tonsteins (such as zircon, sanidine, and monazite) can be used for the determination of radiometric age to identify and correlate coal seams (Lyons et al., 2006; Guerra-Sommer et al., 2008a, b; Wainman et al., 2015; Zhang et al., 2022). The significance of geochemistry and mineralogy of tonsteins can provide useful information to infer regional volcanism events in geology history, the nature of source magmas, depositional conditions of peat accumulation, the subsequent diagenetic processes after coal formation, and regional tectonic evolution of coal-bearing sequences (Dai et al., 2017; Hower et al., 2018, 2022). Moreover, tonsteins in coal-bearing sequences can also enrich some valuable elements and have the potential to recover critical metals (Dai et al., 2017). The leaching by groundwaters/hydrothermal solutions elements from tonsteins into the peat. Thus the underlying or overlying coal benches may enrich some critical elements and then form ore deposits (Crowley et al., 1989; Hower et al., 1999, 2018; Dai et al., 2003, 2017; Zhang et al., 2022). In addition, tonsteins can affect the quality of mined coals by elevating the mineral matter content (Seredin and Finkelman, 2008; Dai et al., 2012a, b, 2017; Seredin and Dai, 2012; Hower et al., 2015).

The Permo-Carboniferous is an important coal-forming interval in geological history, characterized by massive worldwide coal-bearing strata (Liu, 1990; Jiu et al., 2022). Many studies have been carried out on Permo-Carboniferous tonsteins (Zhou et al., 1982; Hess and Lippolt, 1986; Lyons et al., 1992; Webster et al., 1995; Lyons et al., 2006; Guerra-Sommer et al., 2008a, b; Dai et al., 2014a). Many studies have reported the occurrence and age of tonsteins in the Late Paleozoic coals in North China Craton (NCC) (Yang et al., 2006; Pei et al., 2007; Li et al., 2009; Ma et al., 2011; Wang et al., 2011; Luo et al., 2016).

However, combined age-dating with the chemical composition and minerals of the beds have not been studied in detail. Furthermore, the studied areas are located NE margin of the Ordos Basin, the west of NCC and the east of Alxa Terrane (ALT). Therefore, the timing of collision between the NCC and the ALT is not well constrained (Dan et al., 2014, 2016; Yuan and Yang, 2015a, b; Liu et al., 2017). Nevertheless, pyroclastic deposits will be formed by volcanic activities from plate convergence near the plate boundary. Thus, the tonsteins in this study may preserve the NCC-ALT collision event, which can demonstrate the connection between volcanism and tectonic evolution. This paper systematically investigates the features of four tonsteins in the Permo-Carboniferous coal-bearing strata (Benxi Formation) in the northeastern margin of the Ordos Basin in NCC. We provide a relatively precise constraint of the Benxi Formation in NCC, the volcanic origin, and tectonic implications by using petrography, mineralogy, geochemistry, U–Pb isotopic analyses, and Hf isotopic analyses of zircons from the samples. Moreover, we found that tonsteins may affect the concentration of some elements in the surrounding coal seams.

2 Geological background

During the Late Carboniferous to Early Permian, the NCC was in tropical paleolatitudes in the Northern Hemisphere (5-15°N) and bounded by the Sulu orogenic belt to the east, the Central Asian Orogenic Belt (CAOB) to the north, and the Qinling Dabie orogenic belt to the south (Fig. 1b). The eastern segment of the Paleo-Asian Ocean was subducting below its eastern side (the current northern margin). This developed two marginal uplifted orogenic belts to the NCC and gave rise to the E-W-trending tectonic unit of the Inner Mongolia Paleo Uplift (IMPU; Zhang et al., 2007; Torsvik and Cocks, 2019; Wang et al., 2020). Interior cratonic basins of the NCC are filled with terrigenous siliciclastics from the belts and other compression-produced uplifts during the Late Carboniferous to Early Permian (Chen et al., 2020). A large-scale northward transgression occurred in the Late Carboniferous, indicating that the paleogeographical units of the NCC ranged successively from north to south as uplands, alluvial-fluvial plains, paralic deltas, tidal flat-barrier complexes, to shallow-marine environments during the Late Carboniferous to Early Permian (Wang et al., 2020). Furthermore, the widespread formation of distributed pyroclastic deposits preserved now in Carboniferous to Permian coal seams is caused by continuing subduction of the plate and frequent volcanism of the margin of the NCC (Zhang et al., 2007). The Benxi Formation approximately consists of two sedimentary cycles, sandstone to mudstone, limestone and capping coal seams, respectively (Fig. 1d). Late Carboniferous assemblages of fusulinids and conodonts are contained in the two limestone layers, which indicates an age of Late Carboniferous (Wang et al., 1999; Chen et al., 2020).

The strata in the northwest margin of NCC are well exposed and preserved and have many coal and mudstone layers. The Benxi Formation is located in the NE margin of the Ordos Basin, the west of NCC and the east of Alxa Terrane (ALT) (Fig. 1a).

3 Samples and analytical techniques

3.1 Samples

We selected the representative tonstein samples in our collection for this study. Four samples were collected vertically throughout the Benxi Formation in Fugu Section, designated as HZM-1 to HZM-4 from bottom to top (Fig. 1c; Fig. 2). In addition, the HZM-1 and HZM-4 are in coal beds of No. 10 and No. 8, respectively (Fig. 1c; Fig. 2). These samples were examined in the following analytical techniques.

3.2 Analytical techniques

3.2.1 Whole-rock major and trace element analysis

The major analyses of the four tonstein samples were completed in Beijing Qingchen Huanyu Petroleum Geological Technology Co. LTD. Prior to analysis for major element oxides (SiO_2, TiO_2, Al_2O_3, Fe_2O_3, MnO, MgO, CaO, Na_2O, K_2O, and P_2O_5), the powdered tonstein samples were ashed at a temperature of 815 °C for 2.5 h in an inductive oven and used the residues to determine the content of major-element oxides by X-ray fluorescence spectrometry (XRF). Trace elements in the tonsteins were determined using an inductively coupled plasma mass spectrometer (ICP-MS, Agilent 7500a). A mixture of concentrated nitric acids, hydrofluoric acids, and hydrochloric acids was used to dissolve the powdered sample, followed by the approach reported by Dai et al. (2011). All samples were crushed and ground to less than 200 mesh, and about 50 mg of powdered sample was weighed into a Teflon beaker. Then subjected to digestion using mixed acid reagents consisting of 1.5 ml HF and 1.5 ml HNO_3 in an oven at 190°C for 48h. The solution was at ~140°C to dryness, then added 1 ml HNO_3 and evaporated to the second round of dryness. Using ~3 ml of 30% HNO_3 redissolved the solution and then resealed and heated in the bomb at ~190°C for 12-24h. Diluted to about 100g with a mixture of 2% HNO_3 for the final solution. The trace element analyses were completed at the Petroleum Geology Research and Laboratory Center (RIPED).

3.2.2 Zircon U–Pb geochronology

Tonstein samples were collected from the Benxi Formation. After crushing, grinding, sieving, and heavy liquid and magnetic separation, euhedral zircon crystals with clear oscillatory zoning under the cathodoluminescence (CL) microscope were selected for morphology analysis and U–Pb zircon isotope analysis. U–Pb dating was conducted at the Shandong Provincial Key Laboratory of Depositional Mineralization and Sedimentary Minerals, Shandong University of Science and Technology, using a Thermo Fisher's X-Series 2 ICP-MS instrument to acquire ion-signal intensities. Data Cal and Isoplot 3.0 software were used for the age analysis, calculation, and drawing Concordia diagrams from the ICP-MS data. Further details of this technique are given by Lu et al. (2021).

3.2.3 Zircon Hf isotopic analyses

Using a Neptune Plus MC-ICP-MS instrument (Thermo Scientific) to *situ* analyze Hf isotopes in zircon, which needs to combine with a RESOlution M-50193 nm laser ablation (LA) system (Resonetics) at Guangzhou Institute of Geochemistry, Chinese Academy of Sciences (GIGCAS). A further detailed description of the two instruments is given by Zhang et al. (2014), and the data generation process was followed by Zhang L et al. (2015). Twenty-nine analyses of Plešovice zircon yielded a weighted mean $^{176}Hf/^{177}Hf = 0.2824782 \pm 0.0000040$ (2σ), consistent with the value reported by Slama et al. (2008).

3.2.4 Mineralogical analysis

The identification of the morphological features and occurrence modes of the four tonstein samples was carried out using two scanning electron microscopes (SEM) combined with an energy dispersive X-ray spectrometer (EDS) in the Shandong Provincial Key Laboratory of Depositional Mineralization and Sedimentary Minerals, Shandong University of Science and Technology. The mineralogy of the tonsteins was also investigated using powder X-ray diffraction (XRD). The samples were ground to less than 200 mesh using a tungsten carbide mill prior to XRD analysis. The powdered samples were prepared as back-filled mounts to scan from 5 to 70° 20 with 0.02° steps. In addition, the clay (< 2 um) fractions of the samples were separated by ultrasonic dispersion in water with sodium hexametaphosphate (Calgon) and by subsequent settling for 2 h. The clay fractions were placed evenly on glass slides and then scanned in an air-dried state, then after saturation with glycol overnight and after heat treatment at 450°C for 2.5 h. Quantitative mineralogical interpretation was determined by the software SiroquantTMdeveloped by Taylor (1991) following the refinement principles of Rietveld (1969). Further details of this method are given by Dai et al. (2018).

4 Results

4.1 Mineralogy

As the XRD result shows, the tonsteins are composed of kaolinite (91%–100%) and quartz (0.8%–25%), with small amounts of illite (0–3%) and illite/smectite (0%–6%) (Table S1). Sample HZM-4 has the highest kaolinite (99.2%) and lowest quartz (0.8%). Sample HZM-1 has the lowest kaolinite (71.5%) and highest quartz (23.6%). Some kaolinites are found as a well-ordered crystal structure occurring as vermicular aggregates (Fig. 3a, b), confirming the evidence of a volcanic origin (Ruppert and Moore, 1993; Spears, 2012; Dai et al., 2017; Hower et al., 2018). The results of polarized optical microscope observations are consistent with the XRD analysis of samples. For example, the kaolinite in the tonsteins occurs as a cryptocrystalline matrix that surrounds other discrete particles, such as vermicular kaolinite (Fig. 3a, b), muscovite (Fig. 3c, d), potassium feldspar (Fig. 4a), zircon (Fig. 4b), and quartz (Fig. 4c, d). The quartz fragments show angular (Fig. 4c, d), resulting from the pyroclastic origin (Arbuzov et al., 2016; Dai et al., 2017; Shen et al., 2021). Moreover, the euhedral crystals of zircon are frequently present in the tonstein layers.

In addition to the minerals detected by XRD analysis, we also use optical microscopy to observe the minerals. For example, some euhedral crystals of zircon (Fig. 5a, b) have well-developed crystal faces, which may provide evidence of volcanic ash and felsic original ash composition (Arbuzov et al., 2016). Hematite (Fig. 5c, i), ilmenite (Fig. 5d, j), pyrite (Fig. 5e, k), and barite (Fig. 5f, l) were also observed in tonsteins.

4.2 Whole-rock major and trace elements

The results of major element analyses are given in Table S2. The analyzed samples have high SiO_2 (43.86–51.18 wt%) and Al_2O_3 (42.98–53.89 wt%), and low K_2O (0.27–0.32 wt%), Na_2O (0.10–0.41 wt%), CaO (0.09–2.12 wt%), and MgO (0.28–0.75 wt%) contents. The P_2O_5 contents range from 0.01 to 0.02 wt%, and MnO contents are negligible. The Fe_2O_3 contents vary from 0.48 to 0.75 wt% and TiO_2 from 0.29 to 0.60 wt%. The TiO_2/Al_2O_3 ratios lie between 0.0062 from 0.014.

Results of trace element and rare earth element analyses are given in Table S3 and Table S4 (on a whole-rock basis). Contents of Cu decrease gradually upward through the profile from sample HZM-1

to HZM-4, whereas U contents increase from sample HZM-1 to HZM-3. Sample HZM-2 has the highest V (103.7 ppm), Rb (17.8 ppm), and Cr (27.6 ppm) contents. Sample HZM-3 has the highest Mo (13.6 ppm).

The total contents of rare earth elements and yttrium (REY) of the tonstein samples vary from 6.8 to 12.7 ppm (Table S4; on a whole-rock basis). The rare earth elements content is generally low, which may be occurred during the chemical reaction of the upper and lower parts of the tonstein layers with the surrounding coal seams. Previous studies have confirmed that some immobile elements (e.g., Y, Th, Nb, and REEs) may become mobile in coal (Dai et al., 2016; Hower et al., 1999).

In the Chondrite normalized REE diagrams, all of the studied samples show enrichment in light REY, negative Eu anomalies (Eu/Eu* = 0.22 to 0.28; and positive Ce anomalies (Ce/Ce* = 1.06 to 2.36) with high elevated LREY concentrations (Fig. 9c). The UCC-normalized (Taylor and McLennan, 1985) REY patterns of the other four tonsteins also show L-type enrichment, strong negative Eu anomalies (Eu/Eu* = 0.35 to 0.47), and positive Ce anomalies (Ce/Ce* = 1.13 to 2.46; Fig. 9b).

4.3 Zircon U–Pb geochronology

Four tonstein samples were selected for zircon U–Pb geochronological analyses (Table S6). Most of the zircon grains are clear, euhedral to subhedral, and have an excellent euhedral morphology with length-to-width ratios >2. In addition, the analyzed zircons show oscillatory magmatic zoning in CL images (Fig. 6a, b). The Th/U ratios of HZM-1, HZM-2, HZM-3, and HZM-4 are 0.46–0.77, 1.6–6.8, 0.58–1.24, and 0.43–1.03, respectively. These features show that the origin of the zircons is magmatic (Hoskin and Schaltegger, 2003).

We used radiometric age determinations on zircons in four tonsteins (HZM-1, HZM-2, HZM-3, and HZM-4) to determine the absolute ages of the Benxi Formation in the Ordos Basin, which indicates the tonsteins are altered volcanic ash falls. Results of zircon U–Pb laser ablation inductively coupled plasma mass spectrometry (ICP-MS) dating are shown in Fig. 6, Fig. 7, and Table S5. In HZM-1, 14 zircon grains were selected for dating using LA-ICP-MS. The zircon grains of HZM-1 show similar $^{206}Pb/^{238}U$ ages ranging from 275.1 ± 3.1 Ma ± to 319.3 ± 3.1 Ma, with a weighted mean age of 298.8 ± 9.6 Ma (MSWD = 2.6, N = 14) (Fig. 6e, f; Table S5). In HZM-2, 15 zircon grains were selected for U–Pb age dating, which showed similar $^{206}Pb/^{238}U$ ages ranging from 273.1 ± 3 Ma to 319.6 ± 3 Ma, with a weighted mean age of 295.8 ± 6.5 Ma (MSWD = 1.7, N = 15) (Fig. 6c, d; Table S5). In HZM-3, 23 zircon grains were selected for dating using LA-ICP-MS. The zircon grains of HZM-3 show similar $^{206}Pb/^{238}U$ ages ranging from 282.8 ± 3 Ma to 304.8 ± 3 Ma, with a weighted mean age of 295.6 ± 3 Ma (MSWD = 2.8, N = 23) (Fig. 7c, d; Table S5). In HZM-4, 15 zircon grains were selected for U–Pb age dating, which showed similar $^{206}Pb/^{238}U$ ages ranging from 285 ± 3.1 Ma to 301 ± 3.1 Ma, with a weighted mean age of 293.9 ± 3.1 Ma (MSWD = 1.9, N = 15) (Fig. 7a, b; Table S5). The result of the U–Pb age date constrains the Benxi Formation to Gzhelian-Asselian, providing a relatively precise chronostratigraphic framework.

4.4 Zircon in-situ Hf isotopic compositions

In-situ Hf isotopic analyses were performed on the same zircons from samples HZM-1 and HZM-2 used for U–Pb dating (Table S6). As a result, zircon grains from samples HZM-1 and HZM-2 have $\varepsilon_{Hf}(t)$ values of -3.7 to +6.3 and -0.5 to +4.3, respectively (Table S6).

5 Discussions

5.1 Evidence for a volcanic origin of the tonsteins

The mineralogical compositions and field characteristics of tonsteins can provide evidence for volcanic origin (Crowley et al., 1989; Dai et al., 2014b, 2017; Arbuzov et al., 2016; Shen et al., 2021). Our field observations indicate that the HZM tonsteins have the following typical features of volcanic origin: 1) four tonsteins in the field are found as thin beds with a pale color; 2) lateral continuity of the region; 3) an absence of cross-bedding and sedimentary layering structures (Fig. 2).

In addition, the presence of mineral compositions in four tonsteins is crucial evidence of volcanic origin, such as high-temperature quartz and euhedral zircon in the clay beds (Bouroz, 1967; Spears, 2012; Dai et al., 2017). In the present study, the HZM samples were dominated by kaolinite (61.2%–99.2%) that was altered from feldspar crystals and volcanic glasses (Table S1). Furthermore, the quartz in altered volcanic ashes is angular in shape and has common splinters, which are extremely different from normal sedimentary mudrocks (Spears, 2012). Original shapes of pyroclastic materials are retained in the quartz crystals of the HZM samples, such as angular shapes (Fig. 4c, d). The tonstein samples also have vermicular kaolinites (Fig. 3a, b) and many euhedral zircon crystals (Fig. 5a, b) with similar U–Pb ages, suggesting that the tonsteins were formed during volcanism. In addition, the presence of muscovite shows that the tonsteins are also affected by some terrigenous debris. However, the low abundance of muscovite indicates a small terrigenous influence in the tonstein samples.

The zircon U–Pb ages of all the samples analyzed samples show different single-age peaks. Sample

HZM-1 was collected at the lower middle part of the Benxi Formation, with a weighted mean $^{206}Pb/^{238}U$ age of 298.8 ± 9.6 Ma. HZM-2 and HZM-3 were collected at the middle and upper adjacent parts of the Benxi Formation, with a weighted mean $^{206}Pb/^{238}U$ age of 295.8 ± 6.5 Ma and 295.6 ± 3 Ma, respectively. Finally, sample HZM-4 was collected at the bottom of the Benxi Formation, with a weighted mean $^{206}Pb/^{238}U$ age of 293.9 ± 3.1 Ma. All of the above indicates that volcanism may have produced the tonsteins in the Benxi Formation in the studied area. In addition, our new age dating results constrain a relatively tight age to the developing chronostratigraphic chart of Permo-Carboniferous terrestrial sediments in the NCC. The Early Permian was a crucial time for the global evolution of tectonism, which was the final supercontinent convergence and closure of the PAO (Golonka and Ford, 2000; Windley et al., 2007). The tectonic event may generate intense volcanism at the surrounding plate boundary, erupting large amounts of pyroclastic deposits. The production of tonsteins in the Benxi Formation was likely caused by this volcanism, and the precise age can help us constrain the timing of tectonic and volcanism. A further detailed discussion of the evolution of tectonism is given in section 5.3.

5.2 Identification of original magma source

The tonsteins can be divided into three groups: felsic tonsteins, intermediate tonsteins, and mafic tonsteins, which can indicate the original magmas of these tonsteins (Zhou et al., 1982, 2000; Dai et al., 2011, 2017; Spears, 2012). The TiO_2/Al_2O_3 ratios of igneous rocks generally decrease with the increased content of SiO_2 of the parent material. In addition, several authors have suggested and used the TiO_2/Al_2O_3 ratio as a useful provenance indicator for volcanic ash classification in coal, which has also been applied for a similar application in epiclastic sediments (Dai et al., 2011; Hower et al., 2015; Arbuzov et al., 2016; Dai et al., 2017). However, we also need to combine other indicators to identify the original magma source of tonsteins (Dai et al., 2017). Even so, typical TiO_2/Al_2O_3 values for corresponding mafic, intermediate, and felsic tonsteins are > 0.08, 0.02-0.08, and < 0.02, respectively (Winchester and Floyd, 1977; Spears and Kanaris-Sotiriou, 1979; Dai et al., 2014b, 2017). In this study, the TiO_2/Al_2O_3 ratios of the studied samples range from 0.0062 to 0.0140, suggesting that the tonsteins in the Benxi Formation were initially sourced from felsic rocks. The HZM samples plot within the felsic origin field in the TiO_2-Al_2O_3 discrimination diagram (Fig. 8a; Spears and Kanaris-Sotiriou, 1979).

In addition, the classification diagram of Zr/TiO_2 against Nb/Y has also been widely used to estimate the origin and classification of tonsteins (Winchester and Floyd, 1977; Dai et al., 2011, 2015a, 2017; Spears, 2012; Arbuzov et al., 2016). It can classify tonsteins by the volcanic nomenclature, such as rhyolitic tonstein. However, in the Zr/TiO_2-Nb/Y diagram, the four tonstein samples in our study plot are far from the rhyolite field (Fig. 8b). This distribution may be caused by the loss of Y owing to the loss of REY-carrier minerals when the upper or lower parts of the tonsteins reacted with the adjacent coal seams or organic-rich mudstone weathering (Möeller, 2000; Dai et al., 2016, 2017). Therefore, the classification diagram of Winchester and Floyd (1977) could not be a reliable provenance indicator for the tonsteins in this study. Ultimately, the diagrams of Nb/Yb-Al_2O_3/TiO_2 and Zr/TiO_2-Al_2O_3/TiO_2 were also used to distinguish between volcaniclastic deposits of different origin provenance (Shen et al., 2021; Zhang et al., 2022). The U–Pb ages of the zircon grains in the tonsteins of the Benxi Formation indicate that the original volcanic eruption occurred in the Early Permian. We have used the Late Carboniferous-Early Permian volcanic rocks in NCC to identify the original igneous sources in the plotting Zr/TiO_2-Al_2O_3/TiO_2 and Nb/Yb-Al_2O_3/TiO_2 diagrams. All plots of four tonstein samples are situated in or near the rhyolite fields (Fig. 8c, d), which is consistent with a felsic composition for the tonsteins as deduced earlier. The Zr and Nb in the peat-forming environment may be relatively mobile (Dai et al., 2017 and references therein). Thus the tonstein samples of HZM could be slightly affected by it. The different geochemical processes and their predictable patterns of fractionation have coherent behavior; thus, REY elements have been extensively used as geochemical indicators for the altered volcanic ashes within coals (Hower et al., 1999; Dai et al., 2011, 2014a, 2017; Spears, 2012; Arbuzov et al., 2016). Three-fold partitions of REY are classified as light (LREY: La, Ce, Pr, Nd, and Sm), medium (MREY: Eu, Gd, Tb, Dy, and Y), and heavy (HREY: Ho, Er, Tm, Yb, and Lu) (Seredin and Dai, 2012). Generally, REY concentrations in tonsteins can be normalized to both chondrite (Hower et al., 1999; Dai et al., 2011; Arbuzov et al., 2016) and upper continental crust (UCC; Dai et al., 2014b; Shen et al., 2021). Therein, the UCC-normalized REY distribution patterns can assess the changes during the diagenetic and epigenetic stages of development with three enrichment types: L-type (LaN/LuN > 1), M-type (LaN/SmN < 1, GdN/LuN > 1), and H-type (LaN/LuN < 1) (Seredin and Dai, 2012). Moreover, the REY concentrations and distribution patterns may be another geochemical feature indicator that can infer the possible original magmatic material of the tonsteins (Arbuzov et al., 2016; Dai et al., 2017; Wang et al., 2020; Shen et al., 2021). In our study, the four tonstein samples characteristically have obvious negative Eu anomalies with a relatively distinctive fractionation between LREE and HREE, demonstrating that early Eu-enriched plagioclase crystallization and melt extraction resulted in a felsic magma origin (Fig. 9b, c).

In conclusion, the tonstein samples diagrams of TiO_2/Al_2O_3, Nb/Yb-Al_2O_3/TiO_2, Zr/TiO_2-Al_2O_3/TiO_2, and the distribution patterns of REY in the Benxi Formation of the NCC confirmed that studied samples

have a felsic (rhyolite) composition of the initial volcanogenic material.

5.3 Tectonic implications

The geochemical features of the HZM tonsteins may show a magmatic arc origin. In this study, according to the method of Yang et al. (2012) and Wang et al. (2020), the discrimination diagrams of Th/U–Nb/Hf and Th/Nb–Hf/Th indicates that the tectonic setting is arc-related/orogenic in the HZM tonsteins zircons (Fig. 10). The $\varepsilon_{Hf}(t)$ values range from -3.7 to +6.30, with a mean of -0.05 (Table S6). The values of $\varepsilon_{Hf}(t)$ are mostly negative, which indicates a parental magma was derived from the recycled crustal. Moreover, no intraplate magmatic activity has been reported in the NCC during the earliest Permian. Thus, HZM tonsteins may origined from magmatic arc. By analyzing the magmatic arc distribution around the Benxi Formation during the Early Permian, the Inner Mongolia Paleo-uplift (IMPU) and Central Asian Orogenic Belt (CAOB) are two possible sources in the studied area (Zhang et al., 2007; Wang et al., 2020).

The tonsteins in the Benxi Formation show different geochemical features from the pyroclastic deposits in the IMPU and CAOB, indicating the latter were not the origins. Some studies have demonstrated that IMPU is the origin of pyroclastic rocks in the eastern NCC (Zhang et al., 2007; Wang et al., 2020). The tonstein samples in this study have distinct negative Eu anomalies; however, pyroclastic rocks in the eastern NCC display weak negative Eu anomalies (Zhou et al., 2001; Zhao et al., 2019; Wang et al., 2020). In parallel, the tonsteins in the Benxi Formation have no similar negative $\varepsilon_{Hf}(t)$ values compared to rocks from the magmatic arc in the IMPU (Fig. 6a, b). The distribution characteristics of $\varepsilon_{Hf}(t)$ and Eu anomalies about our tonstein samples are also obviously different from CAOB (Fig. 9b, c; Fig. 11a; Wang et al., 2020). Therefore, if the tonstein in this study erupted from a distant volcano in the CAOB, the distribution patterns of REY with obvious negative Eu anomalies should widely occur in the NCC, which is inconsistent with the known distribution of the tonsteins in the NCC. Wang et al. (2020) also conducted a similar study at Wuda Tuff in NCC, the tonstein bed yielding the Wuda Tuff Flora is 66 cm thick, the tonstein bed yielding the Fugu section in this study is ~5-6cm. Wang et al. (2020) suggested that the tonsteins might have erupted from the magmatic arc on the western margin of the NCC, which also was related to the subduction of the PAO oceanic crust in the Early Permian (Fig. 11b), but need further details to confirm it. This research also can infer the same conclusion, which also can suggest the distribution area of such similar tuff layer is from Wuda area to the NE margin of the Ordos Basin. The distance of potential sources is also closer to the Wuda than the study area, because the tonstein bed in Wuda is much thicker than Fugu section. Furthermore, there are amounts of late Paleozoic magmatic rocks with positive zircon Hf isotopes in the northern Alxa Terrane (Liu et al., 2017 and references therein). Some authors suggested the tectonic environments during the formation of the late Paleozoic magmatic rocks in the Alxa Terrane may be an active continental arc setting (Feng et al., 2013; Peng et al., 2013; Zheng et al., 2014; Liu et al., 2017), therefore, northern Alxa Terrane also may be the source of the early magmatic arc of Benxi Formation in this study. But also need further research to confirm it.

The subduction processes and the timing of the final closure of the PAO have been debated for decades, and considerable progress has been made (Charvet et al., 2011; Eizenhöfer et al., 2015; Zhang X R et al., 2015; Han et al., 2016). Our study suggests that the time of final closure of the Paleo-Asian arc may be after 295.8 ± 6.5 Ma, however, the time is also uncertain and needs to be improved in the future. Because other tectonic settings also can generate such characteristics, such as the magmatic rocks from the continent-continent collision setting and inland magmatism from the magmatic arc. Therefore, it needs further research working to confirm the time of the final closure of the Paleo-Asian arc.

In conclusion, the possibility of magmatic arcs around the Early Permian in the studied area needs to be confirmed by further work. However, the significance of the existence of the above hypothesis in the Benxi Formation in NCC is that the ALT and NCC may be separated by a magmatic arc, which also has important implications for the tectonic evolution of the CAOB, NCC, and ALT, and the final closure time of the Paleo-Asian arc.

5.4 Leaching of the tonsteins within coal seams

Some studies have shown that tonsteins within coal seams have been leached by hydrothermal or groundwater solutions, which can cause the high enrichment of some important trace elements in the underlying and overlying coal benches (Crowley et al., 1989; Hower et al., 1999; Dai et al., 2013, 2014a; Arbuzov et al., 2016, 2018; Spears and Arbuzov, 2019). Crowley et al. (1989) demonstrated that leaching of the tonsteins provided a source for many elements (including Zr, Nb, Th, and Ce) enriched in coal samples taken from directly above and below tonsteins. Zhang et al (2022) showed that Th, U, Nb, Ta, Zr, and Hf tend to be enriched in the overlying and underlying coals, which also found the concentrations decrease with the distance from the tonsteins.

The four tonsteins in this study have been confirmed volcanic origin, in which HZM-1 and HZM-4 exist within coal seams. Therefore, we inferred that HZM-1 and HZM-4 are likely to affect the enrichment of elements around coal seams. Compared with the mean composition of clay shale (Grigor'ev, 2003), the studied tonsteins are characterized by high concentrations of Nb and Ta (Fig. 12).

The elements are likely to be enriched in overlying and underlying coal seams through leaching. Moreover, it is quite possible that Nb and Ta can be enriched in overlying and underlying coal seams through leaching. However, the influence of tonsteins around coals in this study needs further research.

6 Conclusions

Based on mineralogical, geochemical, and zircon U–Pb geochronology analyses of four tonsteins from the Permo-Carboniferous Benxi Formation, Ordos Basin, and North China Craton (NCC), we drew the following conclusions:

1) The typical tonstein characteristics, including thin beds with a pale color, lateral continuity of the region, absence of sedimentary layering structures, corrosion gulfs and angular shapes of quartz crystals, vermicular kaolinites, and euhedral zircons with similar U–Pb ages, suggests a significant pyroclastic origin of the tonsteins within coal seams in the Benxi Formation in the NCC. In addition, a small amount of muscovite and detrital zircon grains reflect a slight terrigenous debris contribution of terrigenous debris for the tonsteins.

2) The geochemical characteristics have confirmed that the initial volcanogenic material of the tonsteins is felsic (rhyolite) compositions. The TiO_2/Al_2O_3 values of tonstein samples are low (<0.02), and the Nb/Yb-Al_2O_3/TiO_2, Zr/TiO_2-Al_2O_3/TiO_2 diagrams plotted in or near the rhyolite field. Moreover, the distribution patterns of REY with pronounced negative Eu anomalies confirmed that the tonsteins have a felsic (rhyolite) composition of the initial volcanogenic material.

3) Zircon U–Pb dating of the tonsteins yielded a weighted mean age from 298.8 ± 9.6 Ma to 293.9 ± 3.1 Ma. This provides a relatively precise constraint on the age of the Benxi Formation in the Ordos Basin. The source of the tonsteins may be volcanic from a magmatic arc along the western margin of the NCC during the Early Permian, implying that the ALT had not amalgamated with the NCC by that time, but needs to be improved in the future. However, the above hypothesis also has significant implications for the tectonic evolution of the CAOB, NCC, and ALT and the final closure time of the Paleo-Asian.

4) Tonsteins within coal seams can cause the high enrichment of some important trace elements in the underlying and overlying coal benches. Compared with the mean composition of clay shale, the studied tonsteins are characterized by high concentrations of Nb and Ta, which may affect the surrounding coal seams elemental concentration.

Acknowledgments

This work was supported by the National Natural Science Foundation of China (41972170, 42102127), Shandong Provincial Natural Science Foundation (ZR2021QD087), Chinese Postdoctoral Science Foundation (2021M702019), SDUST Research Fund (2018TDJH101). We would like to thank two anonymous reviewers for their constructive comments.

References

Arbuzov, S.I., Maslov, S.G., Finkelman, R.B., Mezhibor, A.M., Ilenok, S.S., Blokhin, M.G., and Peregudina, E.V., 2018. Modes of occurrence of rare earth elements in peat from Western Siberia. Journal of Geochemical Exploration, 184: 40–48.

Arbuzov, S.I., Mezhibor, A.M., Spears, D.A., Ilenok, S.S., Shaldybin, M.V., and Belaya, E.V., 2016. Nature of tonsteins in the Azeisk deposit of the Irkutsk Coal Basin (Siberia, Russia). International Journal of Coal Geology, 153: 99–111.

Bohor, B.F., and Triplehorn, D.M., 1993. Tonsteins: altered volcanic-ash layers in coal-bearing sequences. Geological Society of America Special Papers, 285 (44 p).

Bouroz, A., 1967. Correlations des tonsteins d'origine volcanique entre les bassins houillers de Sarre-Lorraine et du Nord-Pas-de-Calais. Compte Rendu Hebdomadaire des Seances de l 'Academie des Sciences Serie D Science Naturelle, Paris, 264: 2729–2732.

Cai, P.R., Wang, T., Wang, Z.Q., Li, L.M., Jia, J.L., and Wang, M.Q., 2020. Geochronology and geochemistry of late Paleozoic volcanic rocks from eastern Inner Mongolia, NE China: Implications for igneous petrogenesis, tectonic setting, and geodynamic evolution of the south-eastern Central Asian Orogenic Belt. Lithos, 362: 105480.

Charvet, J., Shu, L.S., Laurent-Charvet, S., Wang, B., Faure, M., Cluzel, D., Chen, Y., and De Jong, K., 2011. Palaeozoic tectonic evolution of the Tianshan belt, NW China. Science China Earth Sciences, 54(2): 166–184.

Chen, A., Zou, H., Ogg, J.G., Yang, S., Hou, M., Jiang, X., Xu, S., and Zhang, X., 2020. Source-to-sink of Late carboniferous Ordos Basin: Constraints on crustal accretion margins converting to orogenic belts bounding the North China Block. Geoscience Frontiers, 11(6): 2031–2052.

Crowley, S.S., Stanton, R.W., and Ryer, T.A., 1989. The effects of volcanic ash on the maceral and chemical composition of the C coal bed, Emery Coal Field, Utah. Organic Geochemistry, 14(3): 315–331.

Dai, S.F., Guo, W.M., Nechaev, V.P., French, D., Ward, C.R., Spiro, B.F., and Finkelman, R.B., 2018. Modes of occurrence and origin of mineral matter in the Palaeogene coal (No. 19-2) from the Hunchun Coalfield, Jilin Province, China. International Journal of Coal Geology, 189: 94–110.

Dai, S.F., Li, T.J., Jiang, Y.F., Ward, C.R., Hower, J.C., Sun, J.H., Liu, J.J., Song, H.J., Wei, J.P., Li, Q.Q., Xie, P.P., and Huang, Q., 2015a. Mineralogical and geochemical compositions of the Pennsylvanian coal in the Hailiushu Mine, Daqingshan Coalfield, Inner Mongolia, China: Implications of sediment-source region and acid hydrothermal solutions. International Journal of Coal Geology, 137: 92–110.

Dai, S.F., Li, T., Seredin, V.V., Ward, C.R., Hower, J.C., Zhou, Y.P., Zhang, M.Q., Song, X.L., Song, W.J., and Zhao,

C.L., 2014a. Origin of minerals and elements in the Late Permian coals, tonsteins, and host rocks of the Xinde Mine, Xuanwei, eastern Yunnan, China. International Journal of Coal Geology, 121: 53–78.
Dai, S.F., Ren, D.Y., Chou, C.L., Finkelman, R.B., Seredin, V.V., and Zhou, Y.P., 2012a. Geochemistry of trace elements in Chinese coals: a review of abundances, genetic types, impacts on human health, and industrial utilization. International Journal of Coal Geology, 94: 3–21.
Dai, S.F., Ren, D.Y., Hou, X.Q., and Shao, L.Y., 2003. Geochemical and mineralogical anomalies of the late Permian coal in the Zhijin coalfield of southwest China and their volcanic origin. International Journal of Coal Geology, 55(2–4): 117–138.
Dai, S.F., Seredin, V.V., Ward, C.R., Hower, J.C., Xing, Y.W., Zhang, W.G., Song, W.J., and Wang, P.P., 2015b. Enrichment of U–Se–Mo–Re–V in coals preserved within marine carbonate successions: geochemical and mineralogical data from the Late Permian Guiding Coalfield, Guizhou, China. Mineralium Deposita, 50(2): 159–186.
Dai, S.F., Wang, X.B., Zhou, Y.P., Hower, J.C., Li, D.H., Chen, W.M., Zhu, X.W., and Zou, J.H., 2011. Chemical and mineralogical compositions of silicic, mafic, and alkali tonsteins in the late Permian coals from the Songzao Coalfield, Chongqing, Southwest China. Chemical Geology, 282(1–2): 29–44.
Dai, S.F., Ward, C.R., Graham, I.T., French, D., Hower, J.C., Zhao, L., and Wang, X.B., 2017. Altered volcanic ashes in coal and coal-bearing sequences: A review of their nature and significance. Earth-Science Reviews, 175: 44–74.
Dai, S.F., Zou, J.H., Jiang, Y.F., Ward, C.R., Wang, X.B., Li, T., Xue, W.F., Liu, S.D., Tian, H.M., Sun, X.H., and Zhou, D., 2012b. Mineralogical and geochemical compositions of the Pennsylvanian coal in the Adaohai Mine, Daqingshan Coalfield, Inner Mongolia, China: Modes of occurrence and origin of diaspore, gorceixite, and ammonian illite. International Journal of Coal Geology, 94: 250–270.
Dai, S.F., Luo, Y.B., Seredin, V.V., Ward, C.R., Hower, J.C., Zhao, L., Liu, S.D., Zhao, C.L., Tian, H.M., and Zou, J.H., 2014b. Revisiting the late Permian coal from the Huayingshan, Sichuan, southwestern China: Enrichment and occurrence modes of minerals and trace elements. International Journal of Coal Geology, 122: 110–128.
Dan, W., Li, X.H., Wang, Q., Wang, X.C., and Liu, Y., 2014. Neoproterozoic S-type granites in the Alxa Block, westernmost North China and tectonic implications: In situ zircon U–Pb–Hf–O isotopic and geochemical constraints. American Journal of Science, 314(1): 110–153.
Dan, W., Li, X., Wang, Q., Wang, X., Wyman, D.A. and Liu, Y., 2016. Phanerozoic amalgamation of the Alxa Block and North China Craton: Evidence from Paleozoic granitoids, U–Pb geochronology and Sr–Nd–Pb–Hf–O isotope geochemistry. Gondwana Research, 32: 105–121.
Eizenhöfer, P.R., Zhao, G.C., Sun, M., Zhang, J., Han, Y.G., and Hou, W.Z., 2015. Geochronological and Hf isotopic variability of detrital zircons in Paleozoic strata across the accretionary collision zone between the North China craton and Mongolian arcs and tectonic implications. Geological Society of America Bulletin, 127(9–10): 1422–1436.
Feng, J.Y., Xiao, W.J., Windley, B., Han, C.M., Wan, B., Zhang, J.E., Ao, S.J., Zhang, Z.Y., and Lin, L.N., 2013. Field geology, geochronology and geochemistry of mafic–ultramafic rocks from Alxa, China: implications for Late Permian accretionary tectonics in the southern Altaids. Journal of Asian Earth Sciences, 78: 114–142.
Golonka, J. and Ford, D., 2000. Pangean (late Carboniferous–Middle Jurassic) paleoenvironment and lithofacies. Palaeogeography, Palaeoclimatology, Palaeoecology, 161(1–2): 1–34.
Grigor'ev, N.A., 2003. Average concentrations of chemical elements in rocks of the upper continental crust. Geochemistry International, 41(7): 711–718.
Guerra-Sommer, M., Cazzulo-Klepzig, M., Formoso, M.L.L., Menegat, R., and Fo, J.G.M., 2008a. U–Pb dating of tonstein layers from a coal succession of the southern Paraná Basin (Brazil): a new geochronological approach. Gondwana Research, 14(3): 474–482.
Guerra-Sommer, M., Cazzulo-Klepzig, M., Santos, J.O.S., Hartmann, L.A., Ketzer, J.M., and Formoso, M.L.L., 2008b. Radiometric age determination of tonsteins and stratigraphic constraints for the Lower Permian coal succession in southern Paraná Basin, Brazil. 74(1): 13–27.
Han, Y.G., Zhao, G.C., Sun, M., Eizenhöfer, P.R., Hou, W.Z., Zhang, X.R., Liu, Q., Wang, B., Liu, D.X., and Xu, B., 2016. Late Paleozoic subduction and collision processes during the amalgamation of the Central Asian Orogenic Belt along the South Tianshan suture zone. Lithos, 246: 1–12.
Hess, J.C., and Lippolt, H.J., 1986. $^{40}Ar/^{39}Ar$ ages of tonstein and tuff sanidines: new calibration points for the improvement of the Upper Carboniferous time scale. Chemical Geology: Isotope Geoscience Section, 59: 143–154.
Hoskin, P.W., and Schaltegger, U., 2003. The composition of zircon and igneous and metamorphic petrogenesis. Reviews in mineralogy and geochemistry, 53(1): 27–62.
Hower, J.C., Berti, D., Hochella Jr, M.F., and Mardon, S.M., 2018. Rare earth minerals in a “no tonstein” section of the Dean (Fire Clay) coal, Knox County, Kentucky. International Journal of Coal Geology, 193: 73–86.
Hower, J.C., Eble, C.F., and Mastalerz, M., 2022. Petrology of the Fire Clay coal, Bear Branch, Perry County, Kentucky. International Journal of Coal Geology, 249: 103891.
Hower, J.C., Groppo, J.G., Henke, K.R., Hood, M.M., Eble, C.F., Honaker, R.Q., Zhang, W.C., and Qian, D.L., 2015. Notes on the potential for the concentration of rare earth elements and yttrium in coal combustion fly ash. Minerals, 5(2): 356–366.
Hower, J.C., Ruppert, L.F., and Eble, C.F., 1999. Lanthanide, yttrium, and zirconium anomalies in the Fire Clay coal bed, Eastern Kentucky. International Journal of Coal Geology, 39(1–3): 141–153.
Hu, F., Huang, W., Yang, Z.L., Wilde, S.A., Furnes, H., Luo, M.S., and Zhang, K.X., 2020. Geochemistry and zircon U–Pb–Hf isotopes of the Mante Aobao granite porphyry at East Ujimqin Banner, Inner Mongolia: implications for petrogenesis and tectonic setting. Geological Magazine, 157(7): 1068–1086.
Jiu, B., Huang, W.H., and Mu, N.N., 2022. Mineralogy and elemental geochemistry of Permo-Carboniferous Li-enriched coal in the southern Ordos Basin, China: Implications for modes of occurrence, controlling factors and sources of Li in coal. Ore Geology Reviews, 141: 104686.
Li, H.Y., Xu, Y.G., Huang, X.L., He, B., Luo, Z.Y., and Yan, B., 2009. Activation of northern margin of the North China Craton in Late Paleozoic: Evidence from U–Pb dating and Hf isotopes of detrital zircons from the Upper Carboniferous Taiyuan Formation in the Ningwu-Jingle basin. Chinese Science Bulletin, 54(4): 677–686.
Liu, C.F., Xu, M.T., Zhou, Z.G., Wang, G.S., Wu, C., Zhu, Y., Li, H.Y., and Ye, B.Y., 2018. Magmatic history during Late Carboniferous to Early Permian in the North of the central Xing’an-Mongolia Orogenic Belt: a case study of the Houtoumiao pluton, Inner Mongolia. International Geology Review, 60(15): 1918–1939.

Liu, G.H., 1990. Permo-Carboniferous paleogeography and coal accumulation and their tectonic control in the North and South China continental plates. International Journal of Coal Geology, 16(1-3): 73-117.
Liu, Q., Zhao, G.C., Han, Y.G., Eizenhöfer, P.R., Zhu, Y.L., Hou, W.Z., and Zhang, X.R., 2017. Timing of the final closure of the Paleo-Asian Ocean in the Alxa Terrane: constraints from geochronology and geochemistry of Late Carboniferous to Permian gabbros and diorites. Lithos, 274: 19–30.
Lu, J., Wang, Y., Yang, M.F., Shao, L.Y., and Hilton, J., 2021. Records of volcanism and organic carbon isotopic composition ($\delta^{13}C_{org}$) linked to changes in atmospheric pCO_2 and climate during the Pennsylvanian icehouse interval. Chemical Geology, 570: 120168.
Luo, Z.W., Zhang, Z.C., Li, K., Li, J.F., Tang, W.H., and Xu, B., 2016. Petrography, geochemistry, and U–Pb detrital zircon dating of Early Permian sedimentary rocks from the North Flank of the North China Craton: Implications for the Late Palaeozoic tectonic evolution of the eastern Central Asian Orogenic Belt. International Geology Review, 58(7): 787–806.
Lyons, P.C., Krogh, T., Kwok, Y., Davis, D.W., Outerbridge, W.F., and Evans Jr, H.T., 2006. Radiometric ages of the Fire Clay tonstein [Pennsylvanian (Upper Carboniferous), Westphalian, Duckmantian]: A comparison of U–Pb zircon single-crystal ages and $^{40}Ar/^{39}Ar$ sanidine single-crystal plateau ages. International Journal of Coal Geology, 67(4): 259–266.
Lyons, P.C., Outerbridge, W.F., Triplehorn, D., Evans Jr, H.T., Congdon, R.D., Capiro, M., Hess, J., and Nash, W.P., 1992. An Appalachian isochron: A kaolinized Carboniferous air-fall volcanic-ash deposit (tonstein). Geological Society of America Bulletin, 104(11): 1515–1527.
Ma, S.X., Meng, Q.R., and Qu, Y.Q., 2011. A study of detrital zircons of Late Carboniferous-Middle Triassic strata in the northern margin of North China block and its geological implication. Geological Bulletin of China, 30(10): 1485–1500.
Möeller, P., 2000. Rare earth elements and yttrium as geochemical indicators of the source of mineral and thermal waters, In: Hydrogeology of Crystalline Rocks. Springer, pp. 227–246.
Pei, F.P., Xu, W.L., Yang, D.B., Zhao, Q.G., Liu, X.M., and Hu, Z.C., 2007. Zircon U–Pb geochronology of basement metamorphic rocks in the Songliao Basin. Chinese Science Bulletin, 52(7): 942–948.
Peng, R.M., Zhai, Y.S., Li, C.S., and Ripley, E.M., 2013. The Erbutu Ni-Cu deposit in the Central Asian Orogenic Belt: a Permian magmatic sulfide deposit related to boninitic magmatism in an arc setting. Economic Geology, 108(8): 1879–1888.
Rietveld, H.M., 1969. A profile refinement method for nuclear and magnetic structures. Journal of applied Crystallography, 2(2):65-71.
Ruppert, L.F., and Moore, T.A., 1993. Differentiation of volcanic ash-fall and water-borne detrital layers in the Eocene Senakin coal bed, Tanjung Formation, Indonesia. Organic Geochemistry, 20(2): 233–247.
Seredin, V.V., and Dai, S.F., 2012. Coal deposits as potential alternative sources for lanthanides and yttrium. International Journal of Coal Geology, 94: 67–93.
Seredin, V.V., and Finkelman, R.B., 2008. Metalliferous coals: a review of the main genetic and geochemical types. International Journal of Coal Geology, 76(4): 253–289.
Shen, M.L., Dai, S.F., Graham, I.T., Nechaev, V.P., French, D., Zhao, F.H., Shao, L.Y., Liu, S.D., Zuo, J.P., Zhao J.T., Chen, K., and Xie, X.H., 2021. Mineralogical and geochemical characteristics of altered volcanic ashes (tonsteins and K-bentonites) from the latest Permian coal-bearing strata of western Guizhou Province, southwestern China. International Journal of Coal Geology, 237: 103707.
Spears, D.A., 2012. The origin of tonsteins, an overview, and links with seatearths, fireclays and fragmental clay rocks. International Journal of Coal Geology, 94: 22–31.
Spears, D.A., and Arbuzov, S.I., 2019. A geochemical and mineralogical update on two major tonsteins in the UK Carboniferous Coal Measures. International Journal of Coal Geology, 210: 103199.
Spears, D.A., and Kanaris- Sotiriou, R., 1979. A geochemical and mineralogical investigation of some British and other European tonsteins. Sedimentology, 26(3): 407–425.
Su, B.X., Qin, K.Z., Sun, H., Tang, D.M., Sakyi, P.A., Chu, Z.Y., Liu, P.P., and Xiao, Q.H., 2012. Subduction-induced mantle heterogeneity beneath Eastern Tianshan and Beishan: insights from Nd–Sr–Hf–O isotopic mapping of Late Paleozoic mafic–ultramafic complexes. Lithos, 134: 41–51.
Sun, S.S., and McDonough, W.F., 1989. Chemical and isotopic systematics of oceanic basalts: implications for mantle composition and processes. Geological Society, London, Special Publications, 42(1): 313–345.
Taylor, J.C., 1991. Computer programs for standardless quantitative analysis of minerals using the full powder diffraction profile. Powder Diffract 6: 2–9.
Taylor, S.R., and McLennan, S.M., 1985. The Continental Crust: Its Composition and Evolution. Oxford: Blackwell, 312.
Tian, D.X., Yang, H., Ge, W.C., Zhang, Y.L., Chen, J.S., Chen, H.J. and Yun, X.Y., 2018. Petrogenesis and tectonic implications of Late Carboniferous continental arc high-K granites in the Dongwuqi area, central Inner Mongolia, North China. Journal of Asian Earth Sciences, 167: 82–102.
Torsvik, T.H., and Cocks, L.R.M., 2019. The integration of palaeomagnetism, the geological record and mantle tomography in the location of ancient continents. Geological Magazine, 156(2): 242–260.
Wainman, C.,C. McCabe, P.J., Crowley, J.L., and Nicoll, R.S., 2015. U–Pb zircon age of the Walloon Coal Measures in the Surat Basin, southeast Queensland: implications for paleogeography and basin subsidence. Australian Journal of Earth Sciences, 62(7): 807–816.
Wang, F., Chen, F.K., Siebel, W., Li, S.Q., Peng, P., and Zhai, M.G., 2011. Zircon U–Pb geochronology and Hf isotopic composition of the Hongqiyingzi Complex, northern Hebei Province: new evidence for Paleoproterozoic and late Paleozoic evolution of the northern margin of the North China craton. Gondwana Research, 20(1): 122–136.
Wang, M., Zhong, Y.T., He, B., Denyszyn, S.W., Wang, J., and Xu, Y.G., 2020. Geochronology and geochemistry of the fossil-flora-bearing Wuda Tuff in North China Craton and its tectonic implications. Lithos, 364: 105485.
Wang, Z.Y., Shang, G.X., and Mao, B.Z., 1999. Fusulinids evolution and coalbed-forming of the Permo-Carboniferous in North China Platform. Earth Science Frontiers, S1: 73–79 (in Chinese with English abstract).
Webster, J.D., Congdon, R.D., and Lyons, P.C., 1995. Determining pre-eruptive compositions of late Paleozoic magma from kaolinized volcanic ashes: Analysis of glass inclusions in quartz microphenocrysts from tonsteins. Geochimica et Cosmochimica Acta, 59(4): 711–720.
Winchester, J.A., and Floyd, P.A., 1977. Geochemical discrimination of different magma series and their differentiation products using immobile elements. Chemical Geology, 20: 325–343.

Windley, B.F., Alexeiev, D., Xiao, W.J., Kröner, A., and Badarch, G., 2007. Tectonic models for accretion of the Central Asian Orogenic Belt. Journal of the Geological Society, 164(1): 31–47.
Yang, J.H, Cawood, P.A., Du, Y.S., Huang, H., Huang, H.W., and Tao, P., 2012. Large Igneous Province and magmatic arc sourced Permian–Triassic volcanogenic sediments in China. Sedimentary Geology, 261: 120–131.
Yang, J.H., Wu, F.Y., Shao, J.A., Wilde, S.A., Xie, L.W., and Liu, X.M., 2006. Constraints on the timing of uplift of the Yanshan Fold and Thrust Belt, North China. Earth Planetary Science Letters, 246(3–4): 336–352.
Yuan, W., and Yang, Z.Y., 2015a. The Alashan Terrane did not amalgamate with North China block by the Late Permian: evidence from Carboniferous and Permian paleomagnetic results. Journal of Asian Earth Sciences, 104: 145–159.
Yuan, W., and Yang, Z.Y, 2015b. Late Devonian closure of the North Qilian Ocean: evidence from detrital zircon U–Pb geochronology and Hf isotopes in the eastern North Qilian Orogenic Belt. International Geology Review, 57(2), 182-198.
Zhang, L., Ren, Z.Y., Nichols, A.R., Zhang, Y.H., Zhang, Y., Qian, S.P., and Liu, J.Q., 2014. Lead isotope analysis of melt inclusions by LA-MC-ICP-MS. Journal of Analytical Atomic Spectrometry, 29(8): 1393–1405.
Zhang, L., Ren, Z.Y., Xia, X.P., Li, J., and Zhang, Z.F., 2015. IsotopeMaker: A Matlab program for isotopic data reduction. International Journal of Mass Spectrometry, 392: 118–124.
Zhang, S.H., Zhao, Y., Kröner, A., Liu, X.M., Xie, L.W., and Chen, F.K., 2009a. Early Permian plutons from the northern North China Block: constraints on continental arc evolution and convergent margin magmatism related to the Central Asian Orogenic Belt. International Journal of Earth Sciences, 98(6): 1441–1467.
Zhang, S.H., Zhao, Y., Song, B., Hu, J.M., Liu, S.W., Yang, Y.H., Chen, F.K., Liu, X.M., and Liu, J., 2009b. Contrasting Late Carboniferous and Late Permian–Middle Triassic intrusive suites from the northern margin of the North China craton: Geochronology, petrogenesis, and tectonic implications. Geological Society of America Bulletin, 121(1–2): 181–200.
Zhang, S.H., Zhao, Y., Song, B., and Yang, Y.H., 2007. Zircon SHRIMP U–Pb and in-situ Lu–Hf isotope analyses of a tuff from Western Beijing: evidence for missing Late Paleozoic arc volcano eruptions at the northern margin of the North China block. Gondwana Research, 12(1–2): 157–165.
Zhang, X.R., Zhao, G.C., Eizenhöfer, P.R., Sun, M., Han, Y.G., Hou, W.Z., Liu, D.X., Wang, B., Liu, Q., and Xu, B., 2015. Paleozoic magmatism and metamorphism in the Central Tianshan block revealed by U–Pb and Lu–Hf isotope studies of detrital zircons from the South Tianshan belt, NW China. Lithos, 233: 193–208.
Zhang, Z.H., Lv, D.W., Wang, C.S., Hower, J.C., Raji, M., Wang, T.T., Zhang, J.Q., and Yang, Y., 2022. Mineralogical and geochemical characteristics of tonsteins from the Middle Jurassic Yan'an Formation, Ordos Basin, North China. International Journal of Coal Geology, 253: 103968.
Zhao, L., Dai, S.F., Nechaev, V.P., Nechaeva, E.V., Graham, I.T., French, D., and Sun, J.H., 2019. Enrichment of critical elements (Nb-Ta-Zr-Hf-REE) within coal and host rocks from the Datanhao mine, Daqingshan Coalfield, northern China. Ore Geology Reviews, 111: 102951.
Zhao, P., Xu, B., and Zhang, C.H., 2017. A rift system in southeastern Central Asian Orogenic Belt: Constraint from sedimentological, geochronological and geochemical investigations of the Late Carboniferous-Early Permian strata in northern Inner Mongolia (China). Gondwana Research, 47: 342–357.
Zheng, R.G., Wu, T.R., Zhang, W., Xu, C., Meng, Q.P., and Zhang, Z.Y., 2014. Late Paleozoic subduction system in the northern margin of the Alxa block, Altaids: geochronological and geochemical evidences from ophiolites. Gondwana Research, 25(2): 842–858.
Zhou, A.C., Jia, B.W., Ma, M.L., and Zhang, H., 2001. The whole sequences of volcanic event deposits on the north margin of the North China Plate and their features. Geology Review, 47: 175–184 (in Chinese with English abstract).
Zhou, W.X., Zhao, X.C., Fu, D., Sun, J.J., Li, Z.Q., Huang, B.H., and Ge, M.C., 2018. Geochronology and geochemistry of the Carboniferous Ulann Tolgoi granite complex from northern Inner Mongolia, China: Petrogenesis and tectonic implications for the Uliastai continental margin. Geological Journal, 53(6): 2690–2709.
Zhou, Y.P., Bohor, B.F., and Ren, Y.L., 2000. Trace element geochemistry of altered volcanic ash layers (tonsteins) in Late Permian coal-bearing formations of eastern Yunnan and western Guizhou Provinces, China. International Journal of Coal Geology, 44(3–4): 305–324.
Zhou, Y.P., Ren, Y.L., and Bohor, B.F., 1982. Origin and distribution of tonsteins in Late Permian coal seams of southwestern China. International Journal of Coal Geology, 2(1): 49–77.
Zhu, R.K., Xu, H.X., Deng, S.H., and Guo, H.L., 2007. Lithofacies palaeogeography of the Permian in northern China. Journal of Palaeogeography, 9(2): 133–142.

About the first author

WANG Luojing, female, born in 1999 in Linyi City, Shandong Province; graduate student; currently studying at Shandong University of Science and Technology. She is now interested in the study on deep paleoclimate. E-mail: wlj199901@163.com.

About the corresponding author

ZHANG Zhihui, male, born in 1993 in Liaocheng City, Shandong Province; postdoctoral fellow; graduated from Shandong University of Science and Technology and China University of Geosciences, Beijing. He is now interested in the study on the Jurassic paleoclimate. E-mail: zhzhihui@sdust.edu.cn.

Figures

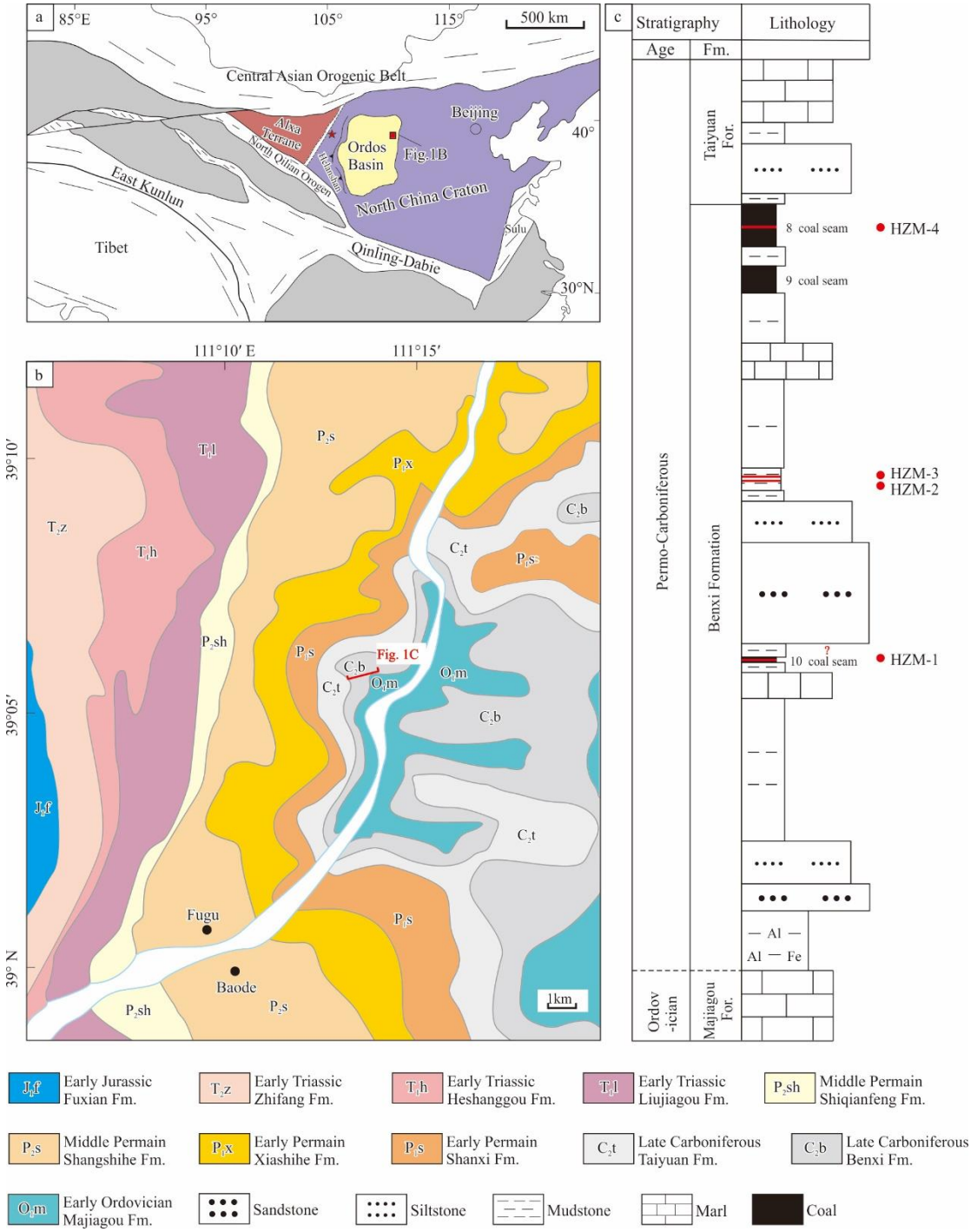

Fig. 1. Location and geology of the study area and stratigraphic column.
(a) Tectonic sketch map of the NCC and adjacent regions from Dan et al. (2016) showing the location of the studied area. The five-pointed star represents the Wuda area; (b) Geological map of the location of the Benxi Formation in the Fugu section (modified from http://www.ngac.org.cn/); (c) Stratigraphic column and sampling locations of the Benxi Formation in the Fugu section, Ordos Basin. For. = Formation.

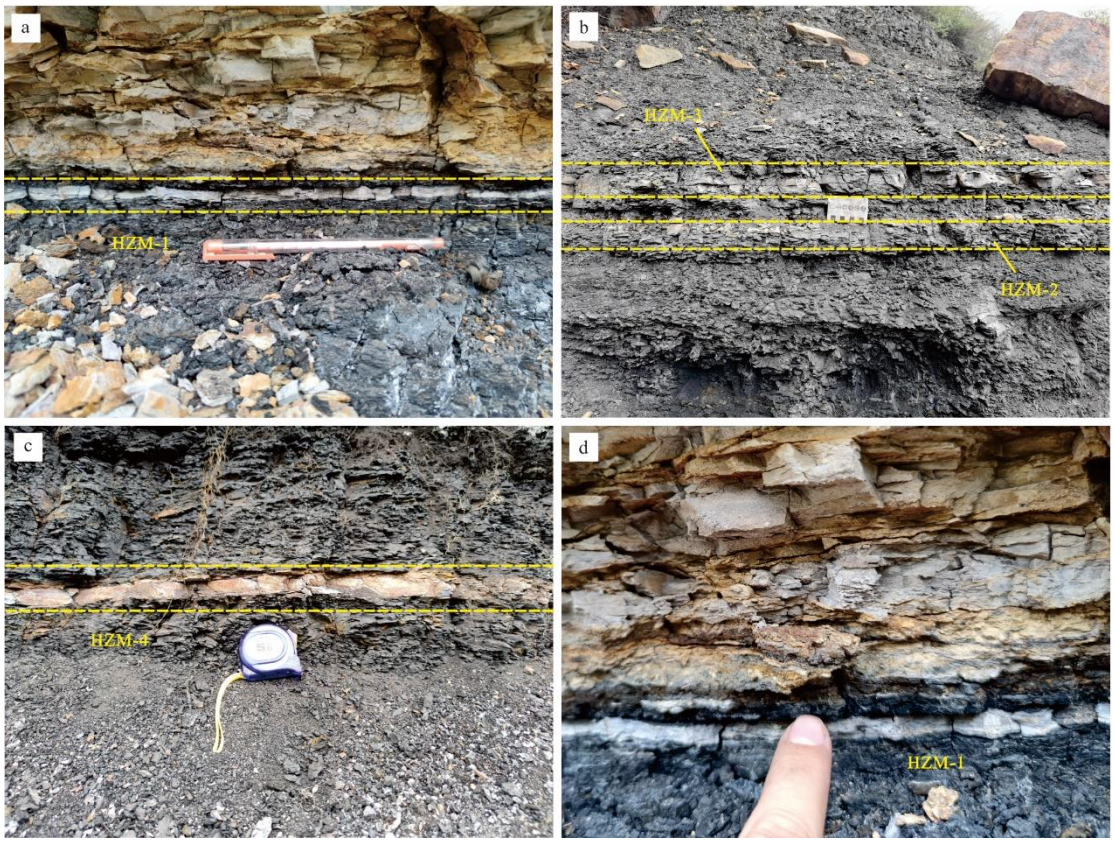

Fig. 2. Field photographs of four tonsteins within coal seams. White thin layers are the tonsteins.

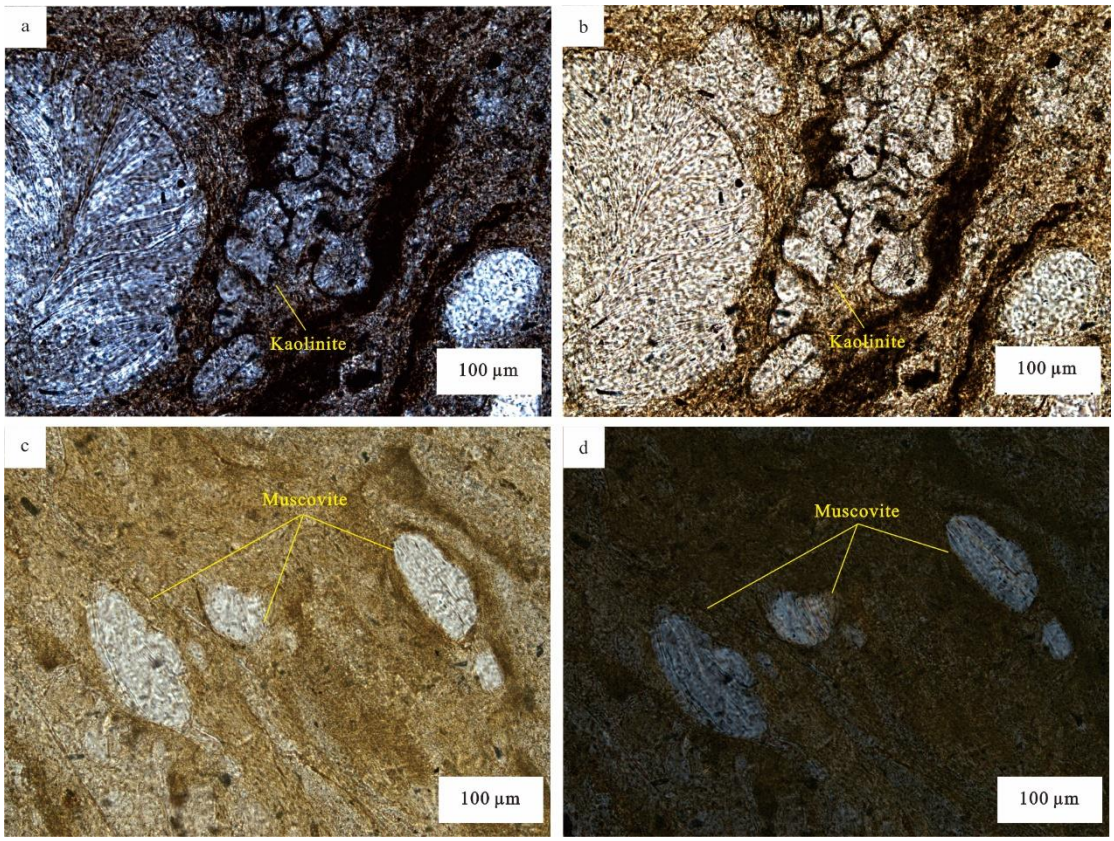

Fig. 3. Petrographic composition of the tonsteins.
(a-b) Vermicular kaolinite of HZM-3, PPL and UXP; (c-d) Muscovite in HZM-4, PPL and UXP.

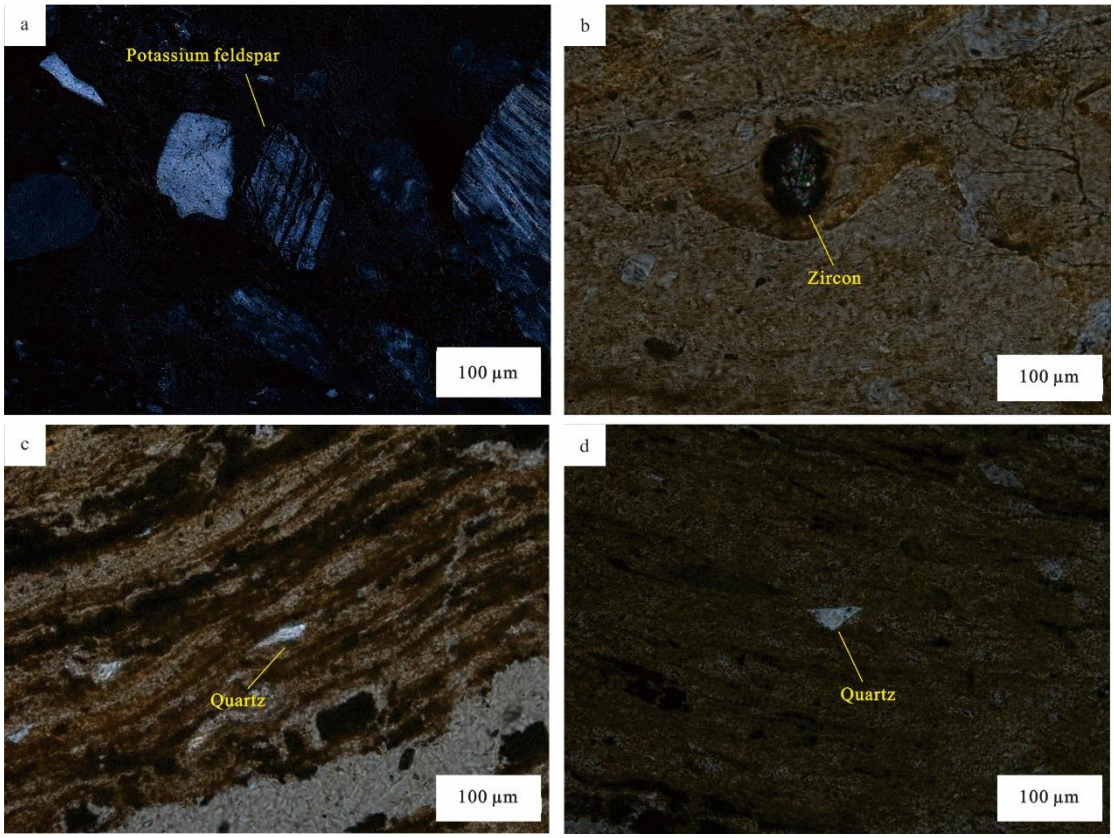

Fig. 4. Petrographic composition of the tonsteins.
(a) Potassium feldspar in HZM-2, UXP; (b) Zircon in HZM-1, UXP; (c-d) Angular quartz in kaolinite matrix of HZM-1 and HZM-2, UXP.

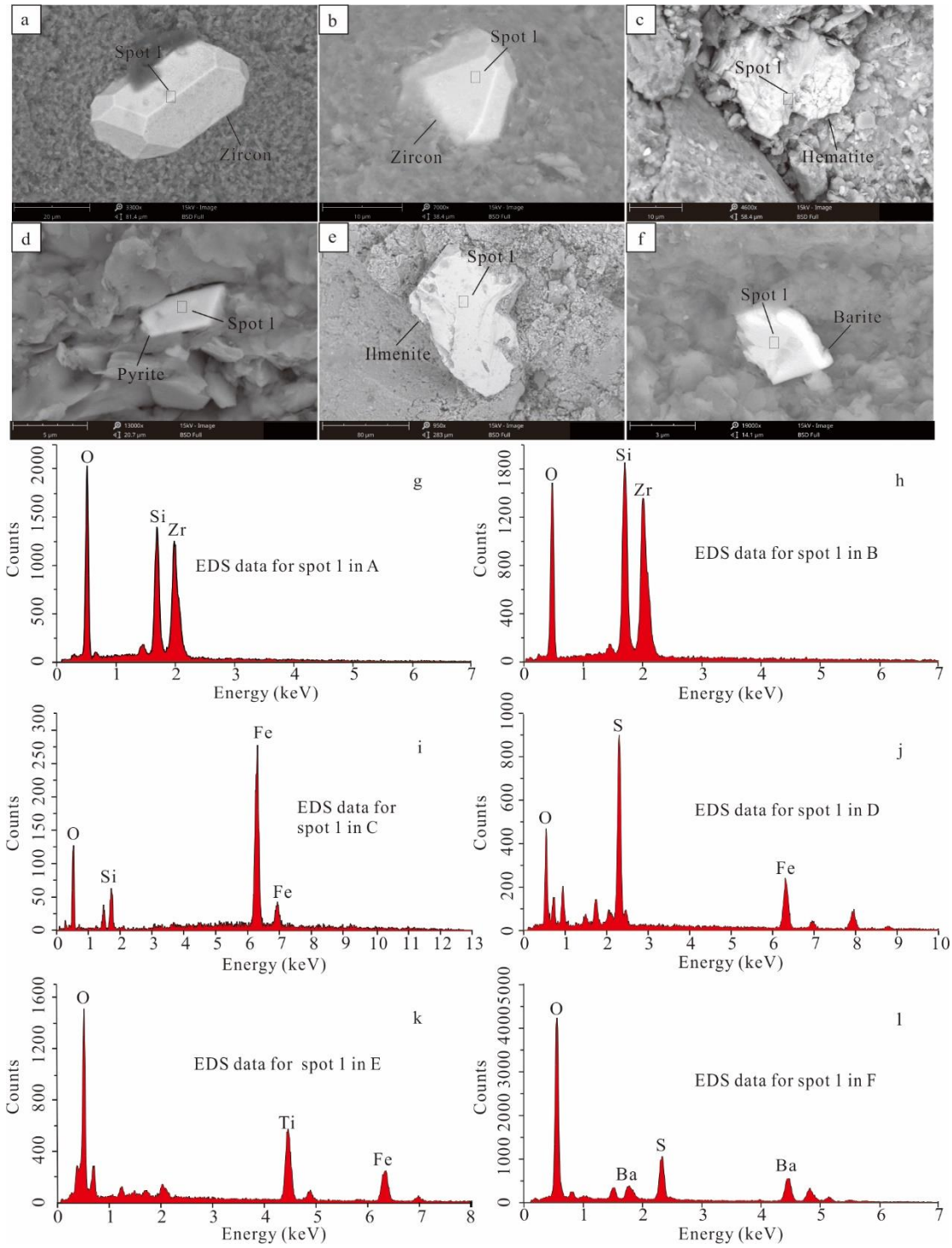

Fig. 5. Representative SEM back-scattered electron image and EDS data of minerals from the studied samples. (a-b) SEM back-scattered electron image of euhedral zircon in HZM-1 and HZM-4; (c) SEM back-scattered electron image of hematite in HZM-2. (d) SEM back-scattered electron image of pyrite in HZM-3; (e) SEM back-scattered electron image of ilmenite in HZM-4; (f) SEM back-scattered electron image of barite in HZM-4; (g-l) EDS data in (a-f), respectively.

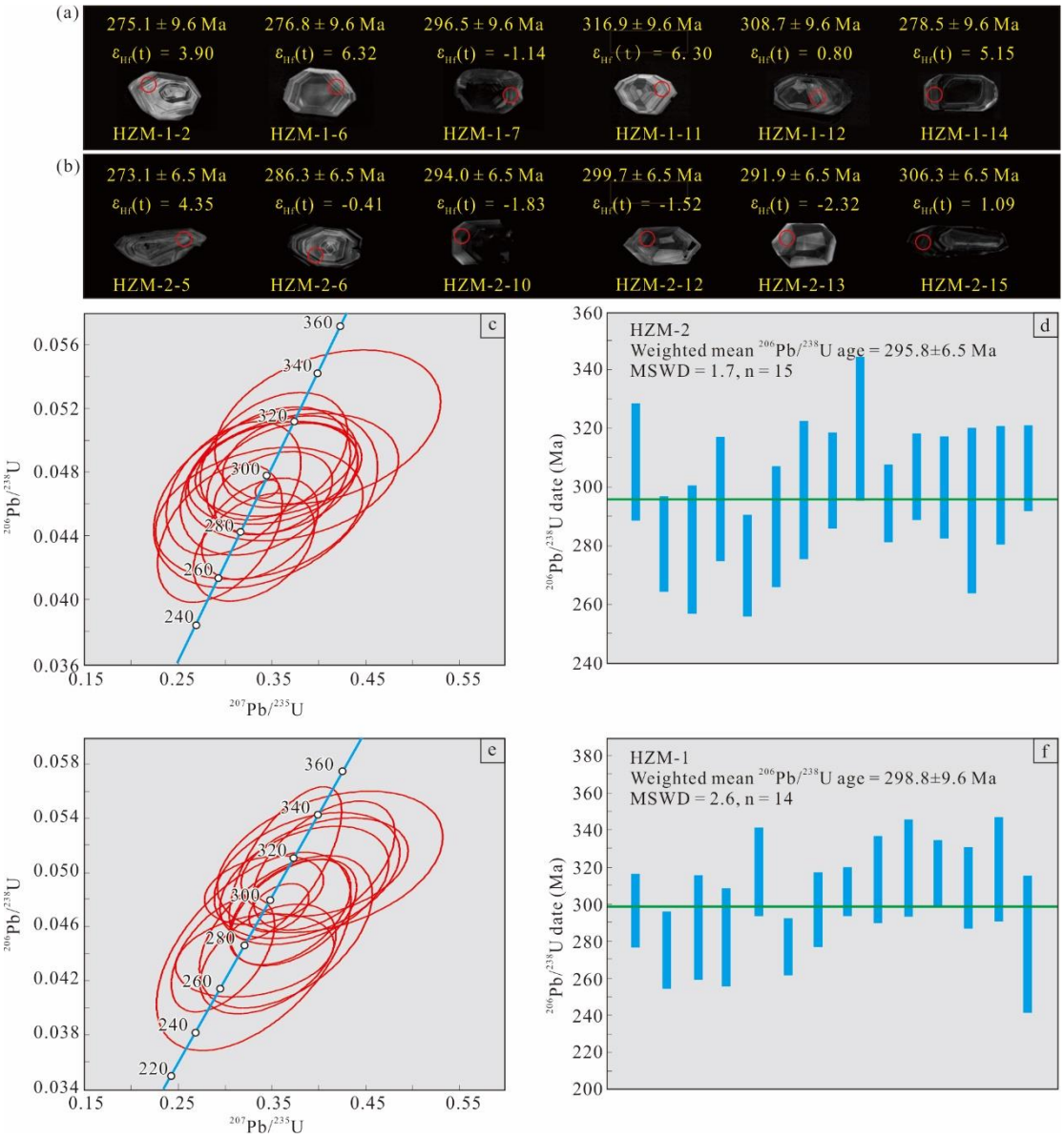

Fig. 6. Cathodoluminescence (CL) images, U–Pb concordia diagrams, and weighted mean age diagrams for zircons from the studied samples.

(a-b) Representative CL images of zircons from tonstein samples HZM-1 and HZM-2; (c-d) zircon U–Pb concordia diagram and calculating weighted mean age for sample HZM-2; (e-f) zircon U–Pb concordia diagram and calculating weighted mean age for sample HZM-1.

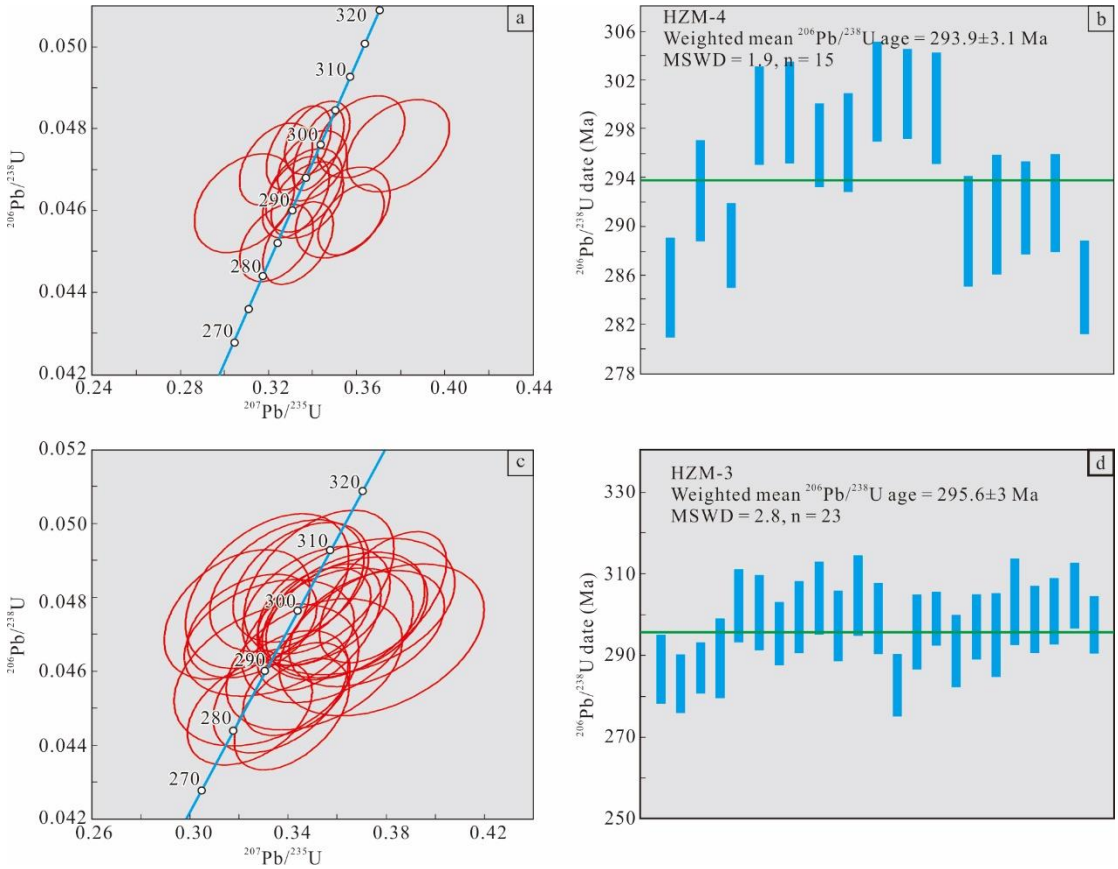

Fig. 7. U–Pb concordia diagrams and weighted mean age diagrams for zircons from the studied samples.
(a-b) zircon U–Pb concordia diagram and calculating weighted mean age for sample HZM-4; (c-d) zircon U–Pb concordia diagram and calculating weighted mean age for sample HZM-3.

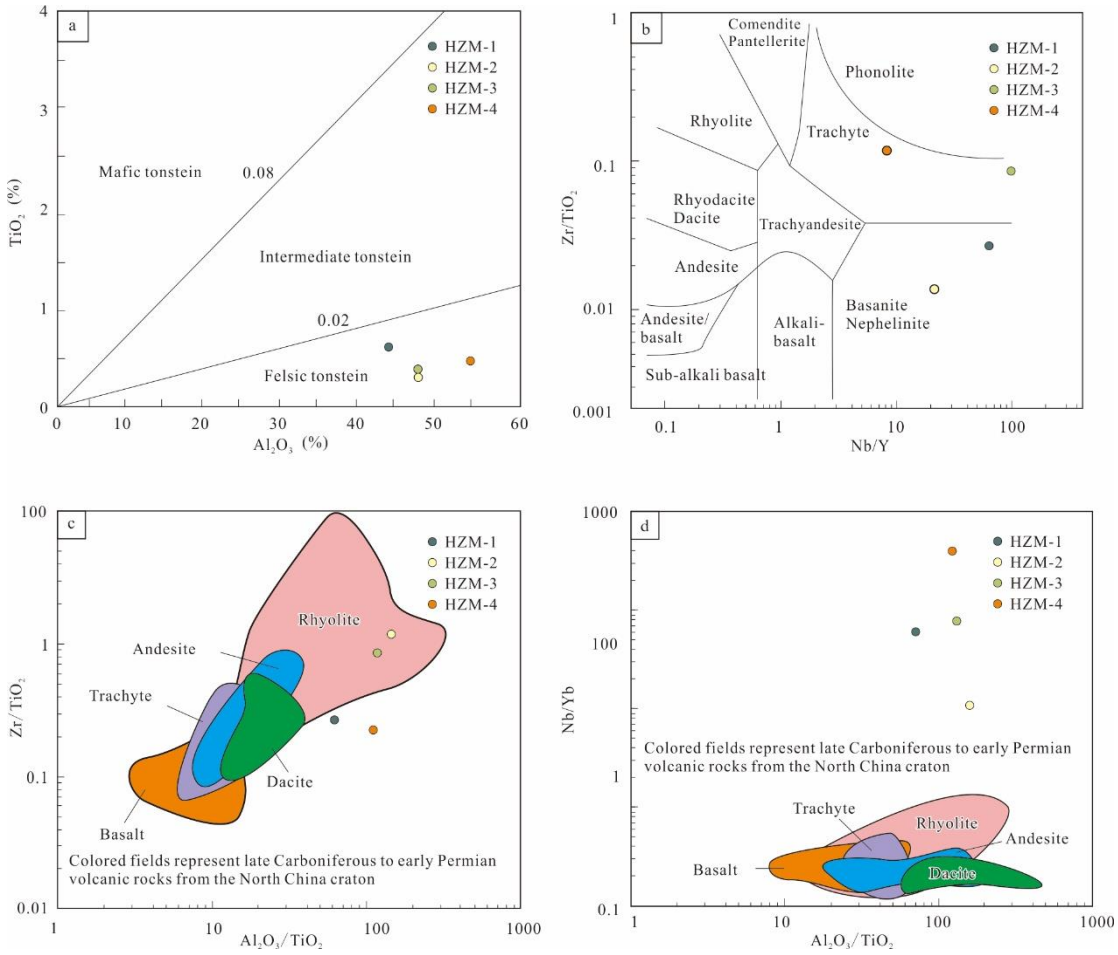

Fig. 8. Discrimination diagrams of the studied samples.

(a) TiO_2-Al_2O_3 discrimination diagram for the HZM tonstein samples (Spears and Kanaris-Sotiriou, 1979). (B) Nb/Y-Zr/TiO_2 classification diagram for the HZM tonstein samples (Winchester and Floyd, 1977); (c-d) The Zr/TiO_2 *versus* Al_2O_3/TiO_2 and Nb/Yb *versus* Al_2O_3/TiO_2 diagrams for the tonsteins. Colored fields represent Late Carboniferous to Early Permian volcanic rocks from the North China craton (Su et al., 2012; Zhao et al., 2017; Liu et al., 2018; Tian et al., 2018; Zhou et al., 2018; Cai et al., 2020; Hu et al., 2020).

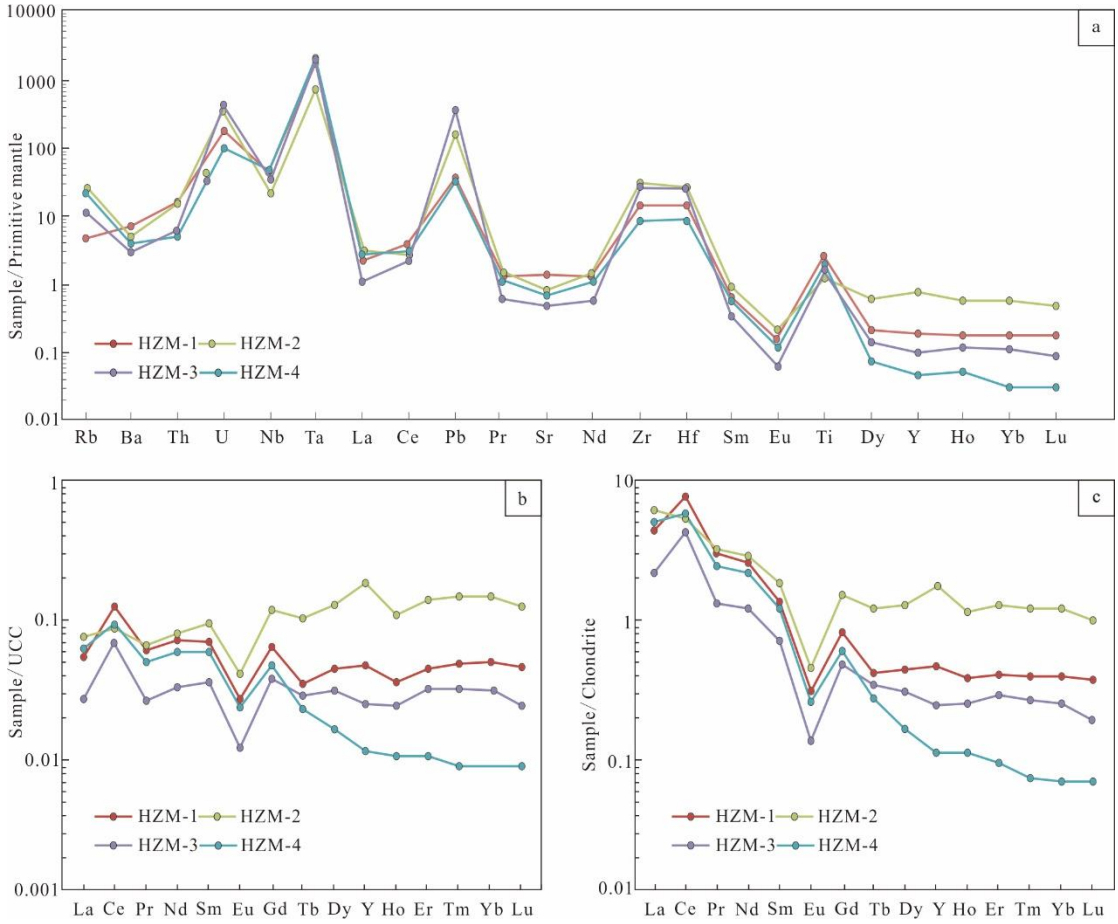

Fig. 9. Normalized element distribution patterns of the studied samples.
(a) Primitive-mantle-normalized trace-element spider diagram. Normalization values are from Sun and McDonough (1989); (b) UCC-normalized REY distribution patterns for the tonsteins. Upper Continental Crust values are from Taylor and McLennan (1985); (c) Chondrite-normalized REY distribution patterns for the tonsteins. Chondrite values are from Taylor and McLennan (1985).

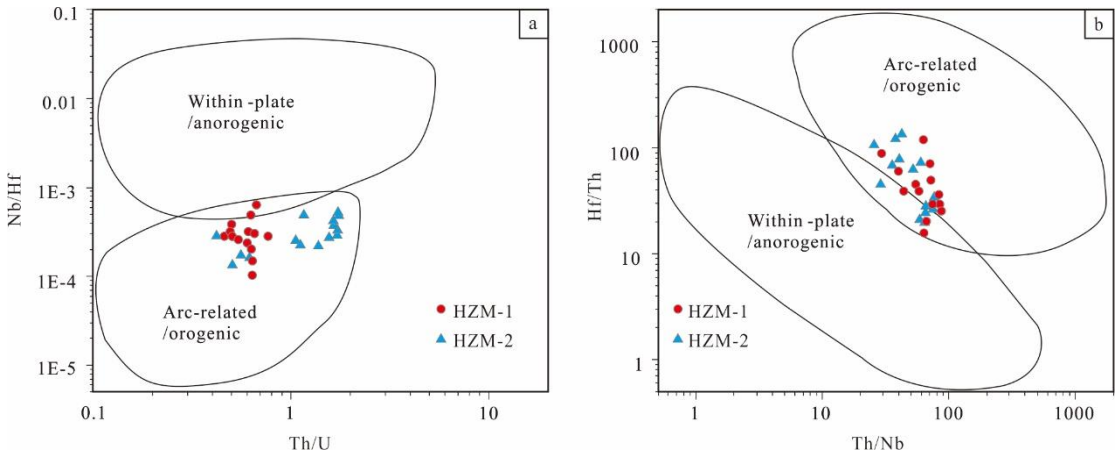

Fig. 10. Th/U–Nb/Hf and Th/Nb–Hf/Th diagrams for tonstein zircons. Modified from Yang et al. (2012).

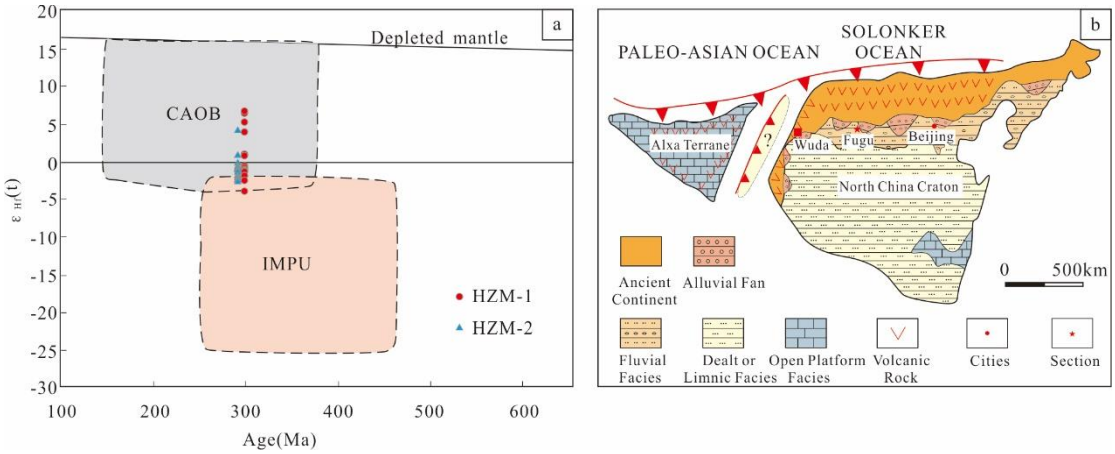

Fig. 11. Compilation diagram of $\varepsilon_{Hf}(t)$ *versus* U–Pb age and paleogeographical map of the North China Craton and Alxa Terrane during the Early Permian.

(a) Compilation diagram of $\varepsilon_{Hf}(t)$ *versus* U–Pb age for the tonsteins from the Benxi Formation in NCC, Central Asian Orogenic Belt (CAOB), and Inner Mongolia Paleo-Uplift (IMPU). Data are compiled from Yang et al. (2006), Zhang et al. (2009a, b), Li et al. (2009), Su et al. (2012), Yuan and Yang (2015b), and Wang et al. (2020); (b) Paleogeographical map of the North China Craton and Alxa Terrane during the Early Permian. Modified from Zhu et al. (2007) and Wang et al. (2020).

Fig. 12. Concentration coefficients (CC = ratios of element concentration in samples vs world clays, Dai et al., 2015b) of trace elements in tonsteins, normalized by the mean composition of clay shale (Grigor'ev, 2003).